THE DIFFUSION AND DECAY OF TURBULENT ELLIPTIC WAKES

by

Yung-huang Kuo and Lionel V. Baldwin

Research Sponsored by the Bureau of Ships
Fundamental Hydromechanics Research Program
Administered by the NONR 1610(08)

Fluid Dynamics and Diffusion Laboratory
College of Engineering
Colorado State University
Fort Collins, Colorado

August 1965 CER65YHK-LVB42

THE DIFFUSION AND DECAY OF TURBULENT ELLIPTIC WAKES

by

Yung-huang Kuo[1] and Lionel V. Baldwin[2]

Fluid Dynamics and Diffusion Laboratory
College of Engineering
Colorado State University
Fort Collins, Colorado

Abstract

Three-dimensional, turbulent wakes having elliptical cross-sections were studied both experimentally and analytically for a constant-fluid-property, zero-pressure-gradient flow. An analytical solution for wake diffusion and decay was obtained from a linearized momentum equation by assuming a constant eddy viscosity in the transverse plane but variable along the wake centerline. The experimental data confirmed the prediction that elliptical wakes approach axisymmetry far downstream. Data were obtained in wakes of 1 inch and 3 inch diameter disks having eccentricities of 1.0, 0.6 and 0.2 over a mean Reynolds number range from 2.4×10^4 to 7.1×10^4. Mean velocity and turbulent intensity data were gathered between 8 and 266 diameters downstream of the disks. Several arbitrary constants of the analysis were determined so that engineering estimates can be made from the analytical results. Unlike axisymmetric and two-dimensional geometries, elliptic wakes offer an opportunity to test eddy

---

1. Research Assistant. Presently Assistant Professor of Civil Engineering, Louisiana State University, Baton Rouge

2. Professor

viscosity assumptions in one plane without adjustable factors, and this was done. However, the mean velocity profiles deviated from the predicted Gaussian shape even though approximate similarity was attained far downstream.

Introduction

The drag of a ballistic projectile imparts momentum to the fluid through which it travels. This induced fluid motion is called the wake of the body and these flow fields have been studied for many years. Much of the recent interest stems from hypersonic missiles and their radar detection from the ionized gas in their wakes (ref. 1). The turbulent structure of a low-speed wake is thought to be a good approximation to the far downstream region of the hypersonic wake. Furthermore, the study of low-speed wakes has its own engineering usefulness in underwater detection schemes.

From the point of view of a research worker in fluid mechanics, elliptic wakes are a tractable version of the general three-dimensional wake problem. The study of elliptic wakes offers a new insight into approximations which must be made to analyze free turbulent shear flows. For this reason, the authors undertook a systematic experimental study of turbulent wakes formed by elliptic disks in a low-speed wind tunnel. The results of this study are summarized in this paper, together with a comparison of the data with the predictions of a theoretical model.

Theoretical Analysis

A comprehensive review of the literature on incompressible wakes up to 1963 was recently published by Halleen (ref. 2). Like all turbulent flows, the formulation of the momentum equations for steady, incompressible, turbulent wakes leads to more unknowns than equations. Analyses

differ then in the assumption used to relate the turbulent shear stresses to the mean flow field. Most wake analyses have focused on the "far" downstream region where the convective acceleration terms can be approximated in a linear manner (an Oseen approximation). Another common feature of most previous analyses is the assumption of similar velocity profiles which reduces the number of independent variables in the partial differential equation. A second common feature is that all solutions require several several empirical constants and naturally, the analyses give no insight into how "far" downstream the predictions are first applicable. Several standard references include a comparison of the solutions for two-dimensional and axisymmetric wakes with available data (e.g., refs. 3, 4 and 5). None of the analyses correctly predict the shape of the mean velocity profile, but several are adequate for estimating purposes.

The analysis for three-dimensional wakes with elliptical cross section published by Steiger and Bloom (refs. 6, 7) is based on the usual simplifying assumptions mentioned above. However, their analysis of the elliptical wake offers several advantages to test eddy diffusivity approximations which are not found in the axisymmetric or two-dimensional geometries. This analysis will be briefly outlined here using the correct definition of wake width (ref. 8) and alternate nondimensional parameters (ref. 9).

The axial momentum equation to be solved is:

$$U_e \frac{\partial \bar{U}}{\partial x} = \frac{\epsilon_\nu}{\rho} \left(\frac{\partial^2 \bar{U}}{\partial y^2} + \frac{\partial^2 \bar{U}}{\partial z^2} \right) \tag{1}$$

Figure 1 is a definition sketch. Equation 1 is derived from the Reynold's averaged, Navier-Stokes equations assuming: steady flow, zero-pressure gradients, negligible transverse velocities and viscous stresses, $U_e >> \bar{U}$, and a constant eddy diffusivity ϵ_ν in the transverse plane to approximate the turbulent shear stress terms. The functional form of ϵ_ν assumed in ref. 7 is a classical one modified slightly to account for three-dimensionality.

$$\epsilon_\nu = 2\ K\ \rho\ \delta_2\ (U_e - U_o) \tag{2}$$

That is, the eddy diffusivity ϵ_ν is directly proportional to the product of defect velocity evaluated at the wake centerline and the wake width along the minor axis. In general, the eddy diffusivity is a function of the axial coordinate x.

The set of nondimensional transform variables used is:

$$\frac{\nu\,(x - x_c)}{U_e\ C_D\ D^2\ B^2} = \int_0^S \frac{\mu}{\epsilon_\nu} \tag{3}$$

$$\sigma = y/\sqrt{C_D}\ DB \quad \text{and} \quad \eta = z/\sqrt{C_D}\ DB \tag{4}$$

$$\phi = \frac{U_e - U}{U_e - U_{oc}} \tag{5}$$

Equation 3 allows the eddy diffusivity ϵ_ν to be a function of the axial position. The new axial coordinate S is defined in a manner that allows the equation of motion to be solved using classical techniques which have been developed for constant diffusivity problems.

The transformed equation of motion is:

$$\frac{\partial \phi}{\partial S} = \frac{\partial^2 \phi}{\partial \eta^2} + \frac{\partial^2 \phi}{\partial \sigma^2} \tag{6}$$

A solution satisfying the usual no flow conditions at infinity and at the initial axial station, $S = 0$ having an assumed Gaussian profile with isovels which have elliptical shape, is:

$$\phi = \frac{\xi}{\left[1 + 4\ S\right]^{1/2}\left[\xi^2 + 4\ S\right]^{1/2}} \exp\left[-\frac{1}{1 + 4\ S}\left\{\eta^2 + \sigma^2\left(\frac{1 + 4\ S}{\xi^2 + 4\ S}\right)\right\}\right] \tag{7}$$

The wake width along the major axis of the ellipse is defined as δ_1

$$z = \delta_1 \text{ when } y = 0 \text{ and } U_e - U = 0.01\,(U_e - U_o) \tag{8}$$

Similarly, the wake width along the minor axis is δ_2 .

$$y = \delta_2 \text{ when } z = 0 \text{ and } U_e - U = 0.01\,(U_e - U_o) \tag{9}$$

Combining equations 2, 3, 7 and 9, the wake growth is predicted as:

$$\delta_2 = \sqrt{C_D}\; DB\,(\ell n\, 100)^{1/2} \left\{ \xi^2 - 1 + \left[(x - x_c)\, \frac{12\,K \left(1 - \frac{U_{oc}}{U_e}\right) (\ell n\, 100)^{1/2}\, \xi}{\sqrt{C_D}\; DB} + 1 \right]^{2/3} \right\}^{1/2} \tag{10}$$

Additional equations can be derived which will be useful later. These are: (a) the wake eccentricity at any dimensionless axial distance S

$$\delta_2 / \delta_1 = \frac{\xi^2 + 4\,S}{1 + 4\,S} \tag{11}$$

Note that at $S = 0$, equation 11 reduces to the definition of ξ ; and (b) the total drag F ,

$$F = \frac{\rho}{2}\; \xi\; \pi\; C_D\; D^2\; B^2\; (U_e - U_{oc})(U_e + U_{oc}) \tag{12}$$

To graphically review the highlights of the analysis figures 2 and 3 were prepared. First, any transverse centerline survey of the mean velocity can be correlated into a single Gaussian profile by proper choice of scale factors. Secondly, the elliptic shape of the wake approaches axisymmetry far downstream as an examination of equation 11 shows. This behavior is illustrated in figure 2. Finally, wake width data should correlate using the variables shown in figure 3 into a single asymptotic curve far downstream, if K and B are true constants and the centerline velocity ratio U_{oc} / U_e is the same from case to case. The asymptotic curve describing wake diffusion is a 1/3-power law which is expected in the axisymmetric case.

There is an array of undetermined factors which must be determined experimentally in order to make specific numerical predictions. Hopefully, a few experiments will suffice to determine these factors: x_c, the virtual origin where the linearized equation first applies; ξ, the eccentricity of the wake at x_c (what relation does ξ have to the body eccentricity?); U_{oc}/U_e, the ratio of the centerline velocity at x_c to ambient velocity; C_D, the drag coefficient of the elliptical body; K, the proportionality factor in the eddy diffusivity formulation; B, a scale factor.

Earlier, the statement was made that "elliptic wakes offer an opportunity to test eddy viscosity assumptions in one plane without adjustable factors." This statement is true in the sense that the factors listed above can be determined from initial station data of the wake's mean velocity configuration at x_c and a measured δ_2 versus x curve. After the factors have been determined it is possible to compare the predicted δ_1 versus x curve with experiments directly. Of course, the "prediction" involves the assumption of constant eddy diffusivity in the transverse plane. A similar assumption is usually made in the axisymmetric and two-dimensional problems without a means of independent check.

Apparatus and Procedure

Wind Tunnel -- The experiments were conducted in a low-speed wind tunnel located in the Fluid Dynamics and Diffusion Laboratory. This tunnel is a recirculating type and has a test section 6 ft. x 6 ft. in cross section and 30 ft. long. An inlet contraction ratio of 4:1 with damping screens yields a free stream turbulence level of less than 2 per cent. The wind tunnel was operated at 58 ft/sec for this research.

A remotely controlled carriage supported the pitot tube and a hot-wire anemometer probe. The position of the probes was sensed by potentiometers which drove the y-axis of a standard x-y plotter.

Disks -- Table 1 shows the dimensions of the disks which were used to generate the wakes. One set had an equivalent frontal area of a 1 inch circular disk, while the other set had the area of a 3 inch circular disk. Each set contained a circular disk and two elliptical disks having eccentricities (ratio of minor to major axis) of $\epsilon = 0.6$ and 0.2 . The disks were made of Lucite plastic and had a sharp edge on the upstream face.

The Reynolds number based on equivalent diameters were 7.1×10^4 and 2.4×10^4 for each set of disks at the operating velocity of 58 ft/sec.

The disks were mounted normal to the air flow at the centerline of the tunnel by piano wire in a diagonal array. For the larger disks, the wire supports were offset in the axial direction to minimize vibration.

Velocity Measurement -- The mean velocity was calculated from total-static pressure from a pitot tube. The pressure difference was converted to an electrical signal for the x-axis of the plotter by a capacitance type of pressure transducer (Trans-sonics Type 120).

Both vertical and horizontal centerline profiles were obtained at 2 ft. axial intervals behind the disk. Several complete surveys of these profiles were taken for each disk. The latter data were used to calculate the disk drag and to test for symmetry. The data extended from 8 to 112 diameters behind the larger disks and from 24 to 266 for the smaller disks.

A constant-temperature, hot-wire anemometer was used to sense the axial turbulent fluctuations in velocity. A spectral analysis of the anemometer signal was performed using two analog circuits: a constant-percentage band-pass analyzer (Bruel and Kjaer Type 2109) and a constant band-pass ($\pm$ 1 cps) analyzer (Technical Products Spectrum Analyzer TP626, 627, 633).

Results and Discussion

Wake Formation -- For all of the disks, a sharp peak was detectable in the measured power spectra of the turbulent velocity within 20 diameters behind the body. The frequency n_p at which the peak in the power spectrum occurred was related to the periodic shedding of vortices at the edge of the disk. The frequency for this periodic motion correlated using a Strouhal number Sl based on free stream velocity U_e and equivalent body diameter D ; that is, $Sl = n_p D/U_e$. Over the Reynolds number range of 8×10^3 to 7×10^4 , Sl = 0.145 for the circular disks, Sl = 0.168 for $\epsilon = 0.6$ and Sl = 0.237 for $\epsilon = 0.2$.

The wake behind the elliptical disks was rotated 90 degrees. The major axis of the wake several body diameters downstream of the body is alined with the minor axis of the body.

More details on the near wake data may be found in references 9 and 10.

Experimental Data on Mean Wake -- The complete set of mean velocity data is summarized in ref. 9. Each disk eccentricity had a characteristic wake development. The profiles near the $\epsilon = 0.2$ disk had off-centerline peaks in the defect velocity $\overline{U}$ which gradually disappeared downstream. The data for each disk approached a similarity profile which seemed distinctive to a given disk eccentricity over the range of these experiments. An example set of the mean velocity data taken at various axial stations is plotted in figure 4. The solid line in figure 4 is the inferred similarity profile for this disk. In like manner, similarity profiles were drawn through the data obtained behind each disk. A summary of these average profiles is given in figures 5 through 8. These plots were prepared using the distances, $Y_{1/2}$ and $Z_{1/2}$, which are experimentally determined lengths where the velocity defect has one-half of its centerline value. Note that in every instance there is systematic deviation from the Gaussian profile which was predicted by the theoretical analysis to be valid for all eccentricities. The deviation of the similarity profiles with body size is puzzling and might be ascribed to the

limited data obtained for the larger disks in the far downstream region where similarity might be expected. In other words, the smaller disk profiles (figs. 6 and 8) are probably more reliable. However, the significant deviation of all the data from the predicted form is evidence of the approximate nature of the theory.

The similarity profiles, which were discussed above, together with the primary data, were used to determine the wake widths δ_1 and δ_2. A summary of these results is given in figures 9 and 10. Note that for a given body size, the data have a systematic variation depending on eccentricity which follows a different sequence for the major and minor axis of the wake. That is, the wake width along the minor axis of the elliptical wake is smaller than the corresponding circular wake, while the major axis data, δ_1, are all larger than the axisymmetric cases. Previous publications (e.g., ref. 1) have suggested that the product $\sqrt{C_D}\ D$ is a characteristic length which, when applied to both the ordinate and abscissa of figures 9 and 10, will correlate the data into a single curve. Although not shown here, this technique did not collapse the elliptical wake data into a common curve.

Figure 11 is a plot of the wake eccentricity. The elliptical wakes approach axisymmetry far downstream as predicted by the analyses. However, it should be emphasized that the body eccentricity for the $\epsilon = 0.6$ disk would plot as 1/0.6 at $x = 0$ and for the $\epsilon = 0.2$ disk at 1/0.2 at $x = 0$. The rotation of the wake is accomplished in a very short distance.

The centerline velocity defect $\overline{U}_o$ is the nondimensionalizing parameter used to form ϕ, the velocity variable in the similarity analysis. The experimentally determined data for $\overline{U}_o$ $\overline{U}_e$ are plotted in figure 12. The scatter is great, but eccentricity of the body appears to be a parameter. The use of $x/\sqrt{C_D}\ D$ as the axial coordinate reduces the systematic deviation of the data with eccentricity, but does not eliminate it.

Evaluation of Constants -- Each of the undetermined constants of the analysis was determined from the six sets of data. A brief summary of these results is given below. There are many alternate ways to determine the

constants from the data, and it is possible to vary the value of some of the "constants" significantly by using various methods. Reference 9 discusses this aspect of the problem in detail. The values presented here were obtained using a self-consistent method which seemed most reliable to the authors for the limited data available.

The drag coefficient C_D was calculated from the velocity defect data by graphical integration at the axial stations where rather complete isovel contour maps could be formed from the profiles. The calculated drag coefficients are plotted in figure 13. The scatter is appreciable because of uncertainty in defining the outer edges of the isovel maps. However, there is no systematic deviation with Reynold's number and a mean value of C_D might be selected for each disk eccentricity. The mean curve from the data of Wieselsberger and Flachsbart (ref. 11) are plotted for comparison of rectangular plate drag with the elliptic disk data.

The value of x_c was determined from each set of velocity defect data by choosing the axial station where the profile data first approximated the similarity profile. For one set of experiments ($\epsilon = 0.2$, $D = 3$ inches), the data did not extend far enough downstream to define the similarity profile accurately. So only five data points are plotted in figure 14. In reference 8, the authors argued that the Oseen approximation for the momentum equation might become valid at a fixed value of the local wake Reynolds number ($\overline{U}_o \, \delta_1 / \nu$). A highly elliptical body ($\epsilon \to o$) would be expected to show a slower rate of decrease of Reynolds number than the circular bodies, because in the limit of a two-dimensional body, the wake Reynolds number is essentially a constant -- independent of axial position. A consequence of this argument is that x_c should increase as the body eccentricity varies from one to zero. The data on figure 14 actually show this trend.

The eccentricity ξ of the wake at the initial station x_c is easily calculated from the data once x_c is determined. The results are summarized in Table 2. The more eccentric disks generated the more elliptic wakes as anticipated, but as noted earlier, the wake is rotated 90 degrees relative to the disk.

The ratio U_{oc} / U_e is the axial velocity at the centerline at the initial station to free stream velocity. This ratio appears in the analytical solution and it too is easily determined from the data once x_c is chosen. Table 2 gives the experimental values. Unfortunately, the slight variation found in this ratio (0.976 to 0.988) is significant in the application of the analytical result, equation 10, because the ratio appears in the equation as the difference from unity.

The scale factor B was determined from the δ_2 data points at the initial station x_c using equation 10. The average value of B is 2.35 ± 0.976.

An average proportionality constant K of the eddy viscosity was calculated from each set of experimental data of δ_2 versus x. Equation 10 was solved for K using the value for δ_2 from each data point where $x > x_c$. An average of the computed K factors was then calculated for each set of wake data; these values are shown in Table 2. For all of the data taken, an average value of K is $8.16 \times 10^{-2} \pm 2.6 \times 10^{-2}$. No systematic deviation with body eccentricity or mean Reynolds number is evident.

The method used to fit the empirical constants involved only data at the initial station x_c (with the exception of some duplicate points for C_D) and the δ_2 data versus x. Therefore, it is of interest to compare the axial variation of the wake widths δ_1 and δ_2 with analytical predictions using the empirical constants adjusted to fit the data at x_c.

This comparison is given in figures 15 through 17. The axisymmetric wake data of figure 15 are adequately described by the calculated curves which are shown for $x > x_c$. From the manner in which the empirical constants were determined, this result was expected for $\epsilon = 1.0$. In figure 16, the wake diffusion behind the $\epsilon = 0.6$ disk is compared with computed curves. In each case, the fit of the δ_2 data is expected but the predicted behavior of δ_1 is less satisfactory. A similar remark describes the approximate fit of the δ_1 data for the most eccentric wake ($\epsilon = 0.2$).

Considering the number of factors involved in the calculation, the fit of the δ_1 data is only fair. However the data are insufficient for large x to test the theory critically.

Although the present experiments did not permit a direct test, the wake behavior very far downstream is predicted in graphical form by figure 18. The shaded area represents the maximum data spread due to experimental uncertainty in B, K and U_{oc} / U_e which were found to vary from case to case. Figure 18 together with mean values of C_D and x_c from figures 13 and 14, might be adequate for engineering estimates on elliptic wakes under some circumstances if the crude assumption of $\xi = \epsilon$ (wake eccentricity at initial station = body eccentricity) is made.

Experimental Data on Wake Turbulence -- Reference 9 gives a more complete tabulation of results than is possible here. Briefly, the turbulent profiles substantiated the finding that the major axis of the wake is alined with the minor axes of the body. The variation of the axial intensity of turbulence along the wake centerline is shown in Figure 19. These data might be useful in formulating alternate forms of the eddy diffusivity.

Concluding Remarks

The experimental study of wakes in a low-speed wind tunnel is difficult because the mean velocity defect is small. The data scatter reflects this problem. However, sufficient evidence does exist to show that the analytical model only gives an estimate of the velocity profiles in the actual wake. With the experimental constants determined in this work, it is possible to make predictions of wake diffusion and decay. Elliptic wakes were alined opposite to the eccentricity of the elliptic body which generated the wake over the range of this experiment.

References

1. Lees, L., "Hypersonic wakes and trials," A.I.A.A. Journal, 2, pp 417-428 (1964).

2. Halleen, R.M., "A literature review on subsonic free turbulent shear flow," Stanford University Report MD-11 (AFOSR-TN-5444). (1964).

3. Goldstein, S., Modern Developments in Fluid Dynamics, Vol. II, Oxford Press, pp. 548-592 (1950).

4. Schlichting, H., Boundary Layer Theory, 4th Ed., McGraw-Hill, pp. 590-631 (1960).

5. Hinze, J.O., Turbulence, McGraw-Hill, pp. 376-447 (1959).

6. Steiger, M.H. and Bloom, M.H., "Three dimensional viscous wakes," Journal of Fluid Mechanics, 14, pp. 233-240 (1962).

7. Steiger, M.H. and Bloom, M.H., "Three-dimensional effects in viscous wakes," A.I.A.A. Journal, 1, pp. 776-782 (1963).

8. Kuo, Y.H. and Baldwin, L.V., "Comments on three-dimensional effects in viscous wakes," A.I.A.A. Journal, 2, pp. 1163-1164 (1964).

9. Kuo, Y.H., "Three-dimensional turbulent wakes," Doctoral Dissertation at Colorado State University (1965).

10. Kuo, Y.H. and Baldwin, L.V., "The formation of turbulent elliptical wakes," paper submitted to the Journal of Fluid Mechanics (1965).

11. Flashsbart, V.O., "Messungen an Ebenen und Gewolbten Platten". Ergenbnisse der Aerodynamicschen Versuchesanstalt zu Gottingen, 4, pp. 96-100, Munich U. Berlin R. Oldenbourg (1932).

12. Cooper, R.D. and Lutzky, M., "Exploratory investigation of turbulent wakes behind bluff bodies," David Taylor Model Basin Report 963 (1955).

13. Hwang, N.H.C. and Baldwin, L.V., "The decay of turbulence in axisymmetric wakes," Transact. A.S.M.E., Series -, J. of Power, (to be published). ASME PAPER 65 - FE 8.

Table 1, Dimensions of disks

Body Eccentricity, ϵ	Equivalent Diameter of Disk, D	Major Axis, inches	Minor Axis, inches	Thickness of disks, inches
1.0	3 inch	3.00	3.00	0.50
	1 inch	1.00	1.00	0.25
0.6	3 inch equivalent	3.88	2.32	0.50
	1 inch equivalent	1.29	0.775	0.25
0.2	3 inch equivalent	6.72	1.34	0.50
	1 inch equivalent	2.24	0.448	0.25

Table 2, Computed characteristic constants for the analytical solution

ϵ	D (in)	X_c (ft)	ξ	U_{oc}/U_e	B	K	C_D
1.0	3	10	1.0	0.976	1.7	0.056	0.938
	1	5	1.0	0.980	2.16	0.0755	1.071
0.6	3	16	0.816	0.982	2.19	0.1078	1.058
	1	6	0.619	0.982	2.6	0.1164	1.124
0.2	3	--	----	----	---	----	1.180
	1	12	0.513	0.988	3.03	0.0524	1.386

LIST OF SYMBOLS

Symbol		Dimension
B	Scale factor, equation (4)	---
C_D	Drag coefficient	---
D	Equivalent diameter	L
F	Body drag	F
K	Proportionality constant of eddy viscosity	---
S	Transformed axial coordinate	---
U	Axial velocity component	L/T
$\bar{U}$	$U_e - U$, Axial velocity defect	L/T
U_e	Free stream velocity	L/T
$\bar{U}_o$	Axial defect velocity at wake center	L/T
$Y_{1/2}$	Width of mean wake behind disk in horizontal direction at which $\bar{U} = \frac{1}{2}\bar{U}_o$	L
$Z_{1/2}$	Width of mean wake behind disk in vertical direction at which $\bar{U} = \frac{1}{2}\bar{U}_o$	L
$\sqrt{\overline{u^2}}$	Root-mean-square of axial turbulent velocity, u'	L/T
δ_1	Wake size in Z direction along major axis of wake; equation (8)	L
δ_2	Wake size in Y direction along minor axis of wake; equation (9)	L
ϵ	Body eccentricity	---
ξ	Wake eccentricity at x_c	---
ϵ_ν	Turbulent eddy viscosity (equation 2)	FT/L^2
ρ	Density of air	FT^2/L^4
σ , η	Transformed normal coordinates; (equation 4) corresponding to Y, Z	---
ϕ	$U_e - U/(U_e - U_{oc})$, Dimensionless axial velocity defect	---

Subscripts

c	Conditions at an initial station
e	Free-stream flow conditions
o	Conditions along the x axis
1/2	Conditions of half-wake width

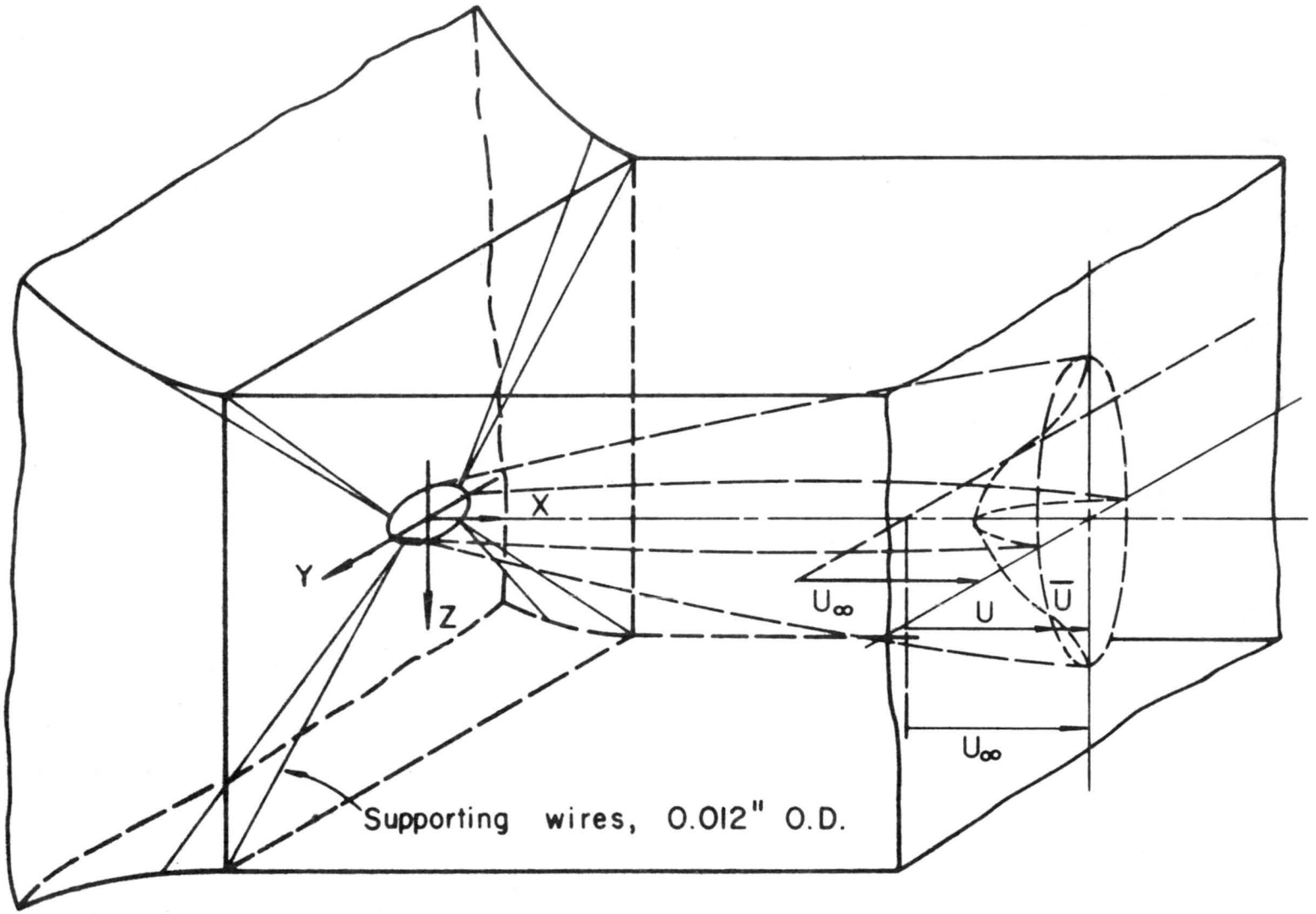

Figure 1. Sketch showing position of the disk in the wind tunnel.

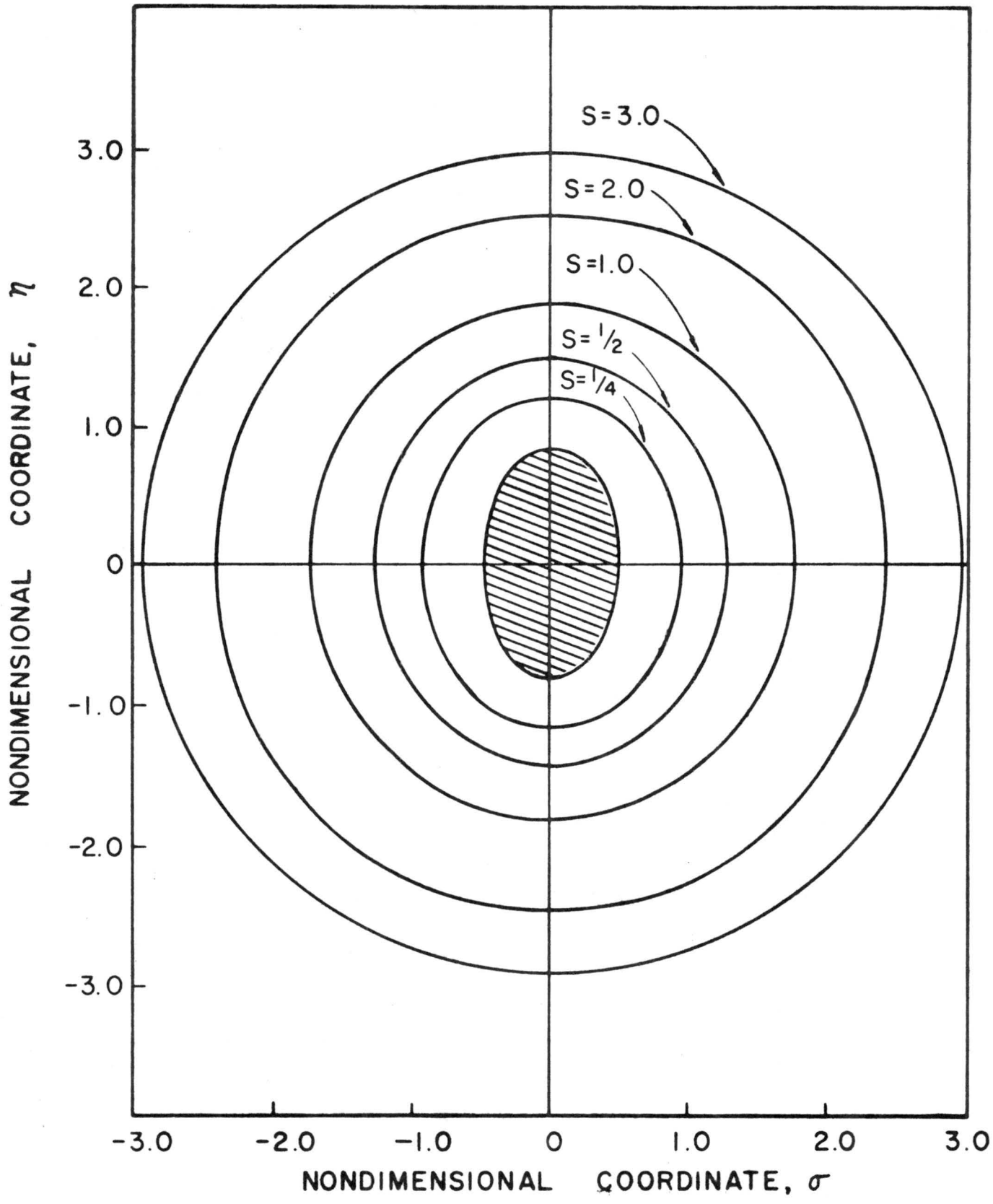

Figure 2. Nondimensional Isovels, $\frac{U_e - U}{U_e - U_o} = 0.5$, at various axial with $\epsilon = 0.6$.

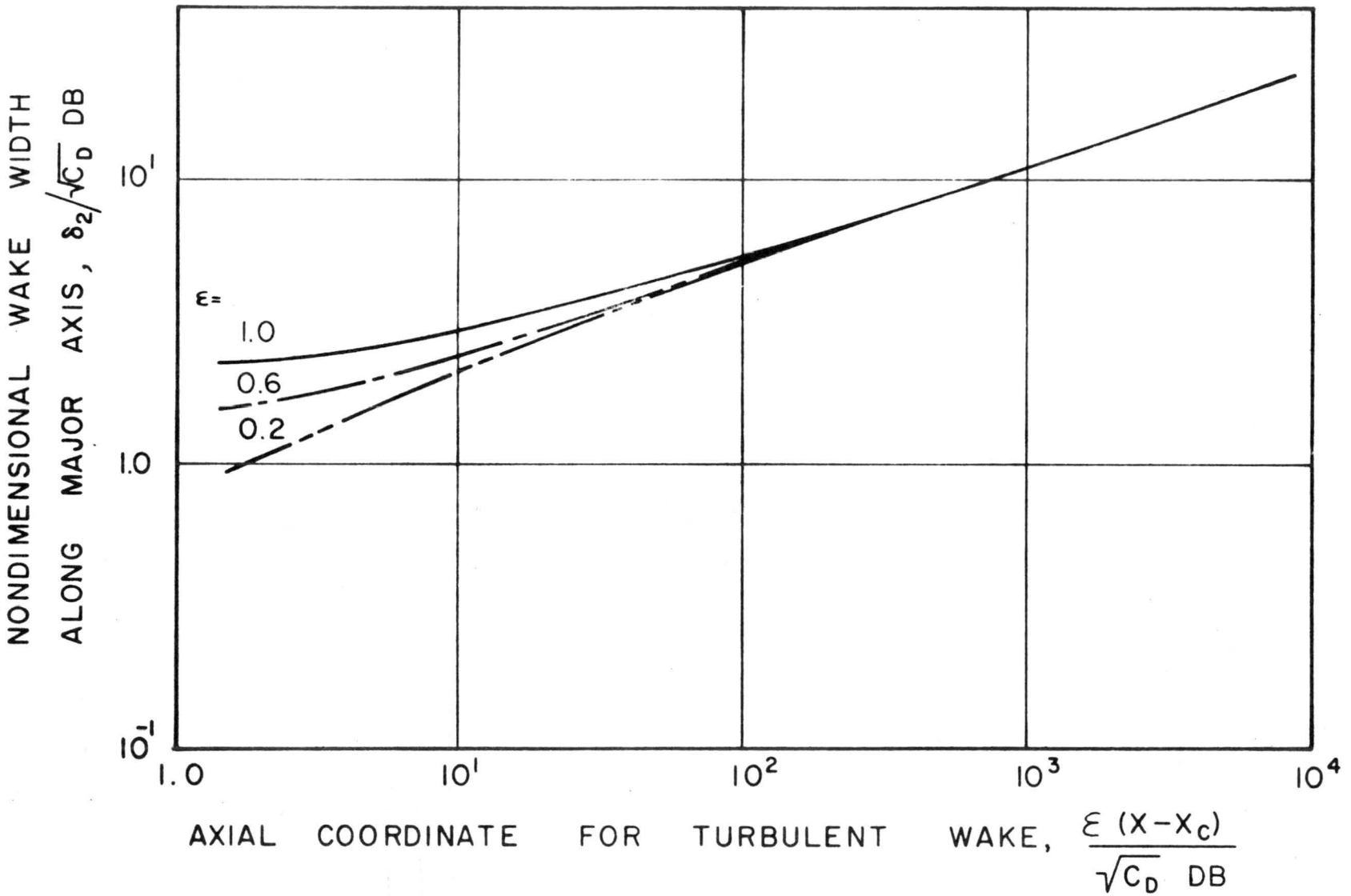

Figure 3. Wake Growth Along Major Axis For Various Values of ξ .
Assumed Constants: $U_{oc} = 0.4\ U_e$, $K = 10^{-2}$

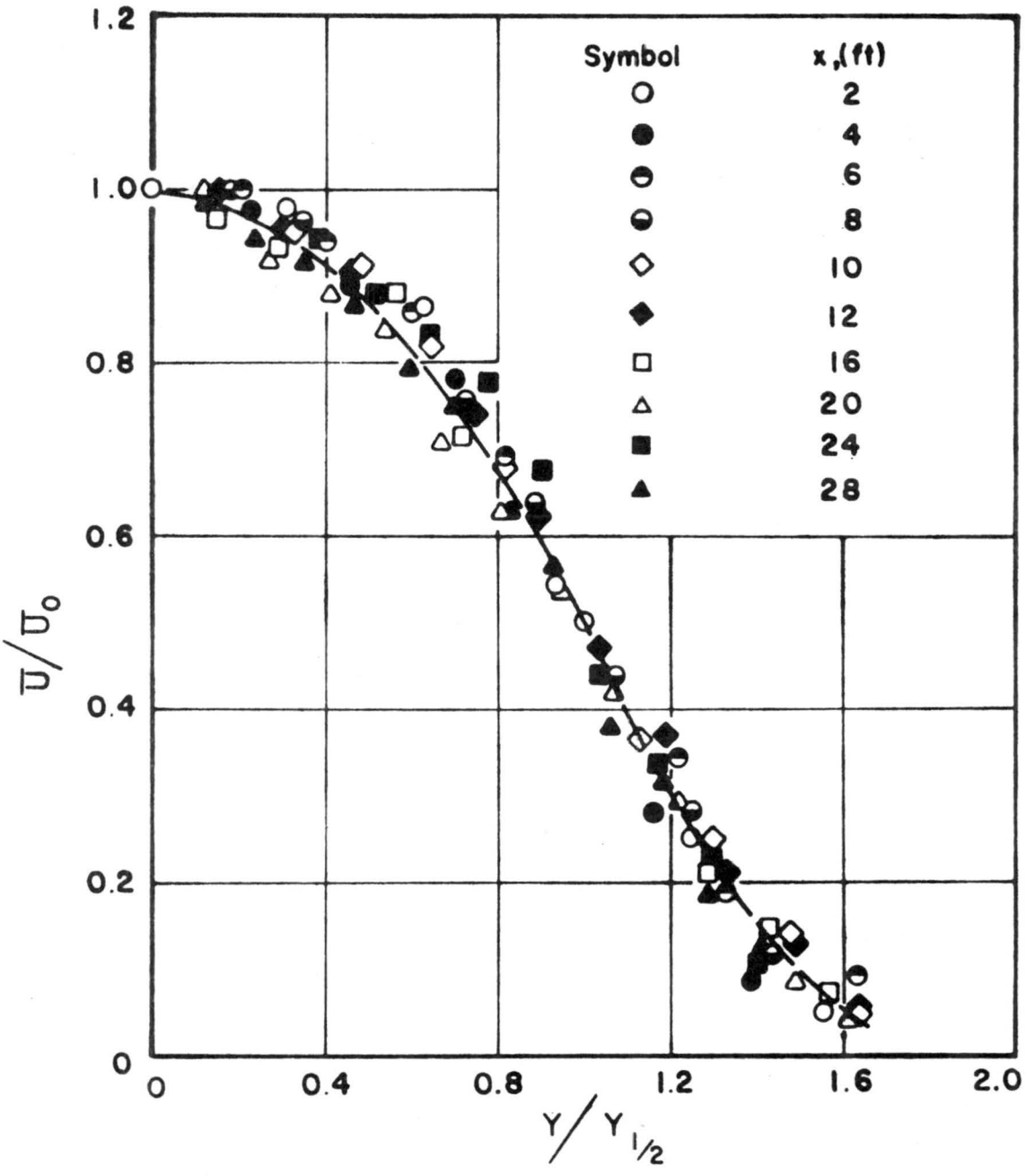

Figure 4. Velocity defect data at various axial stations with inferred similarity profile. D = 3.0 inch, ϵ = 1.0 .

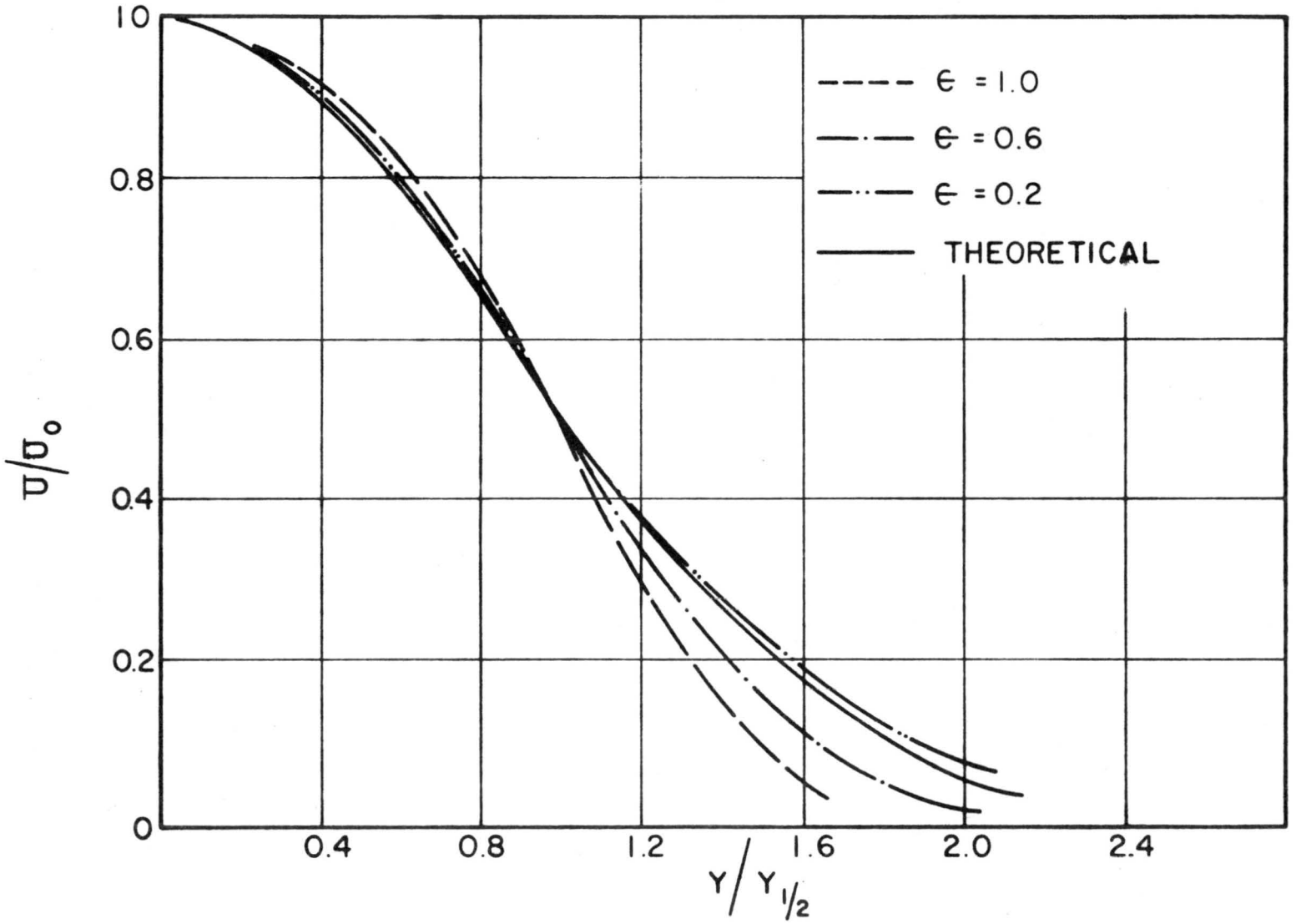

Figure 5. Similarity Velocity Defect Profiles Along Minor Axis of Wake (3 inch Equivalent Diameter Disks)

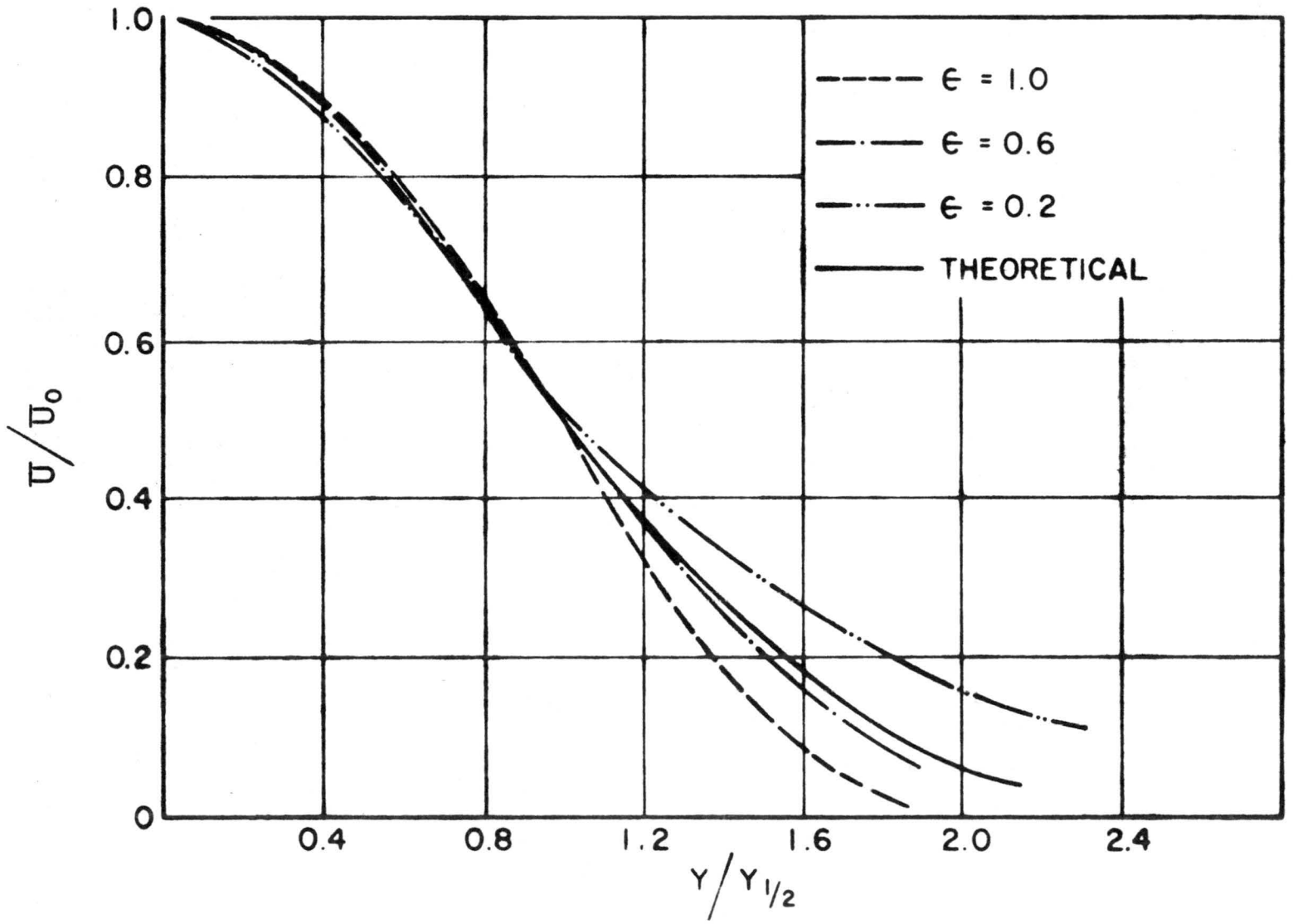

Figure 6. Similarity Defect Velocity Profiles Along Minor Axis of Wake (1 inch Equivalent Diameter Disks)

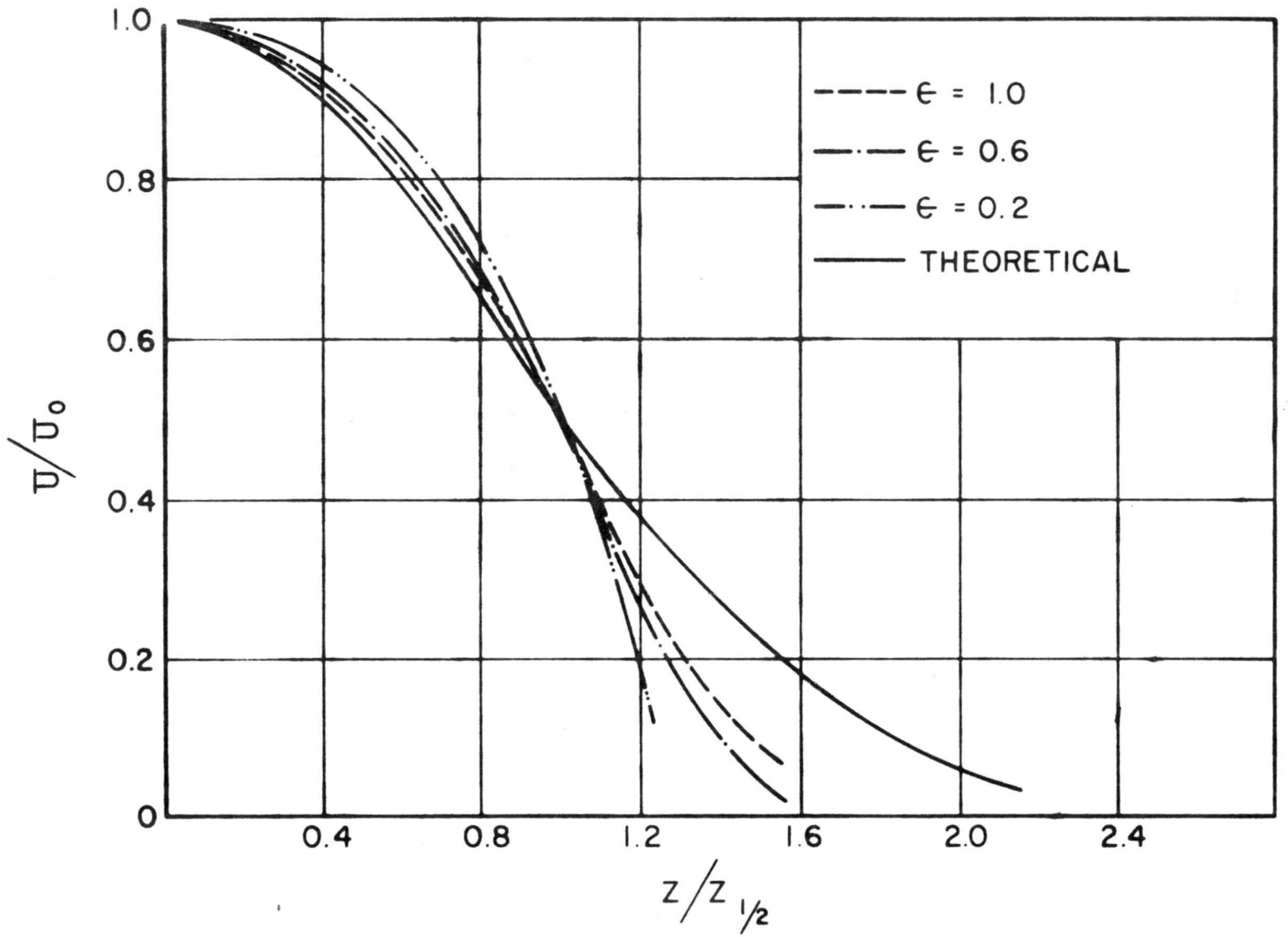

Figure 7. Similarity Defect Velocity Profiles Along Major Axis of Wake (3 inch Equivalent Diameter Disks)

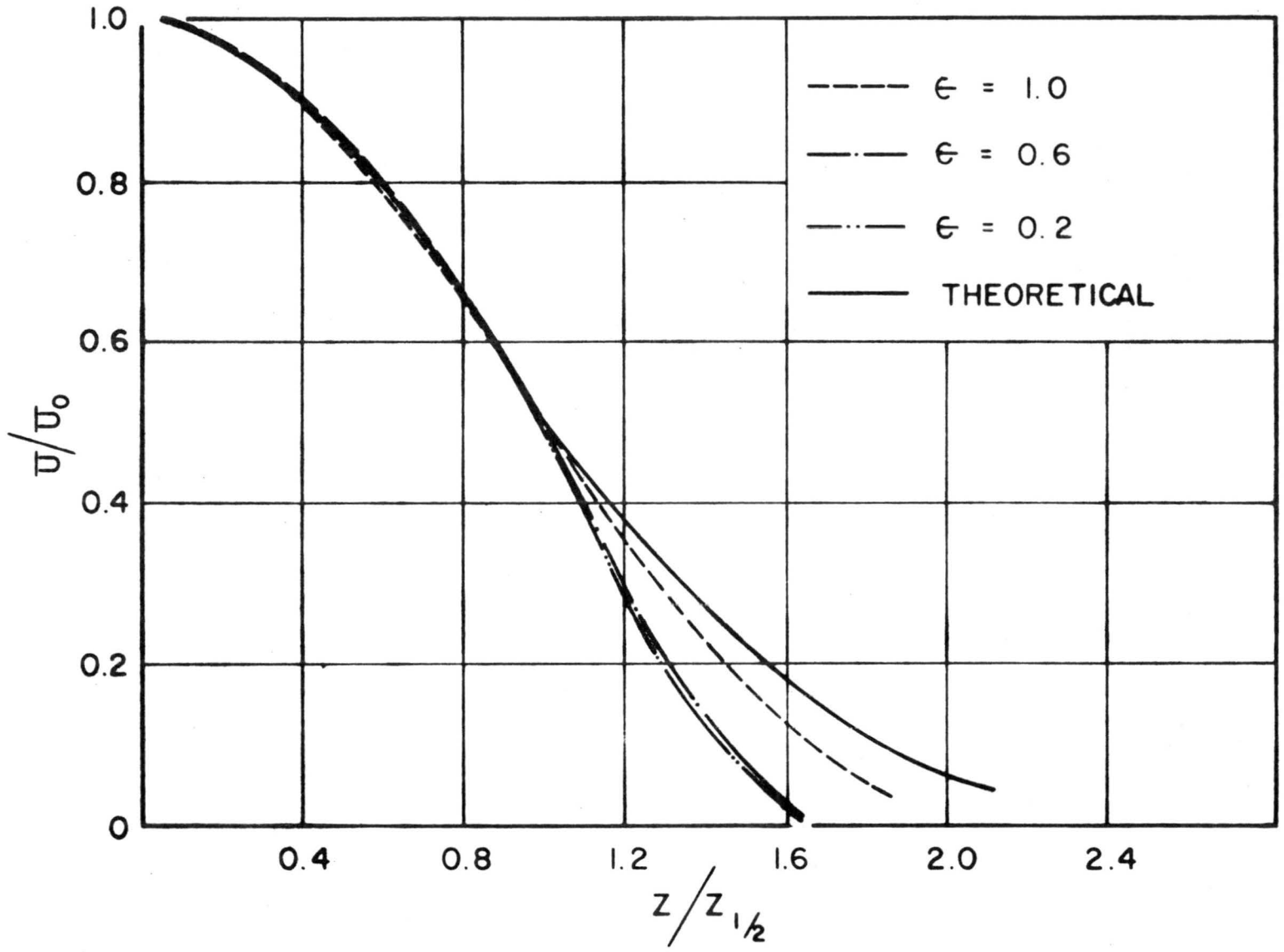

Figure 8. Similarity Defect Velocity Profiles Along Major Axis of Wake (1 inch Equivalent Diameter Disks)

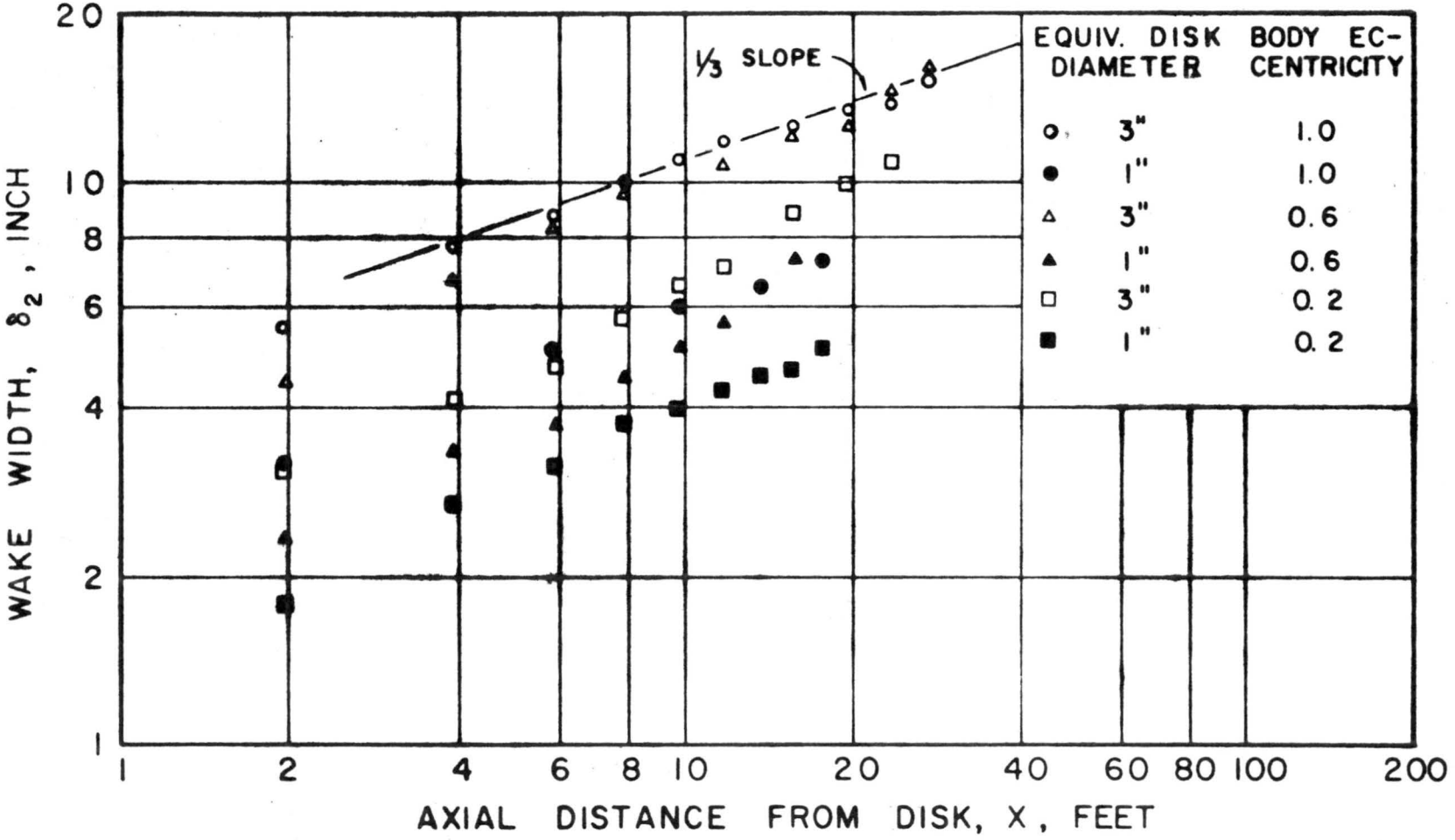

Figure 9. Wake Growth Along the Minor Axis of the Wake.

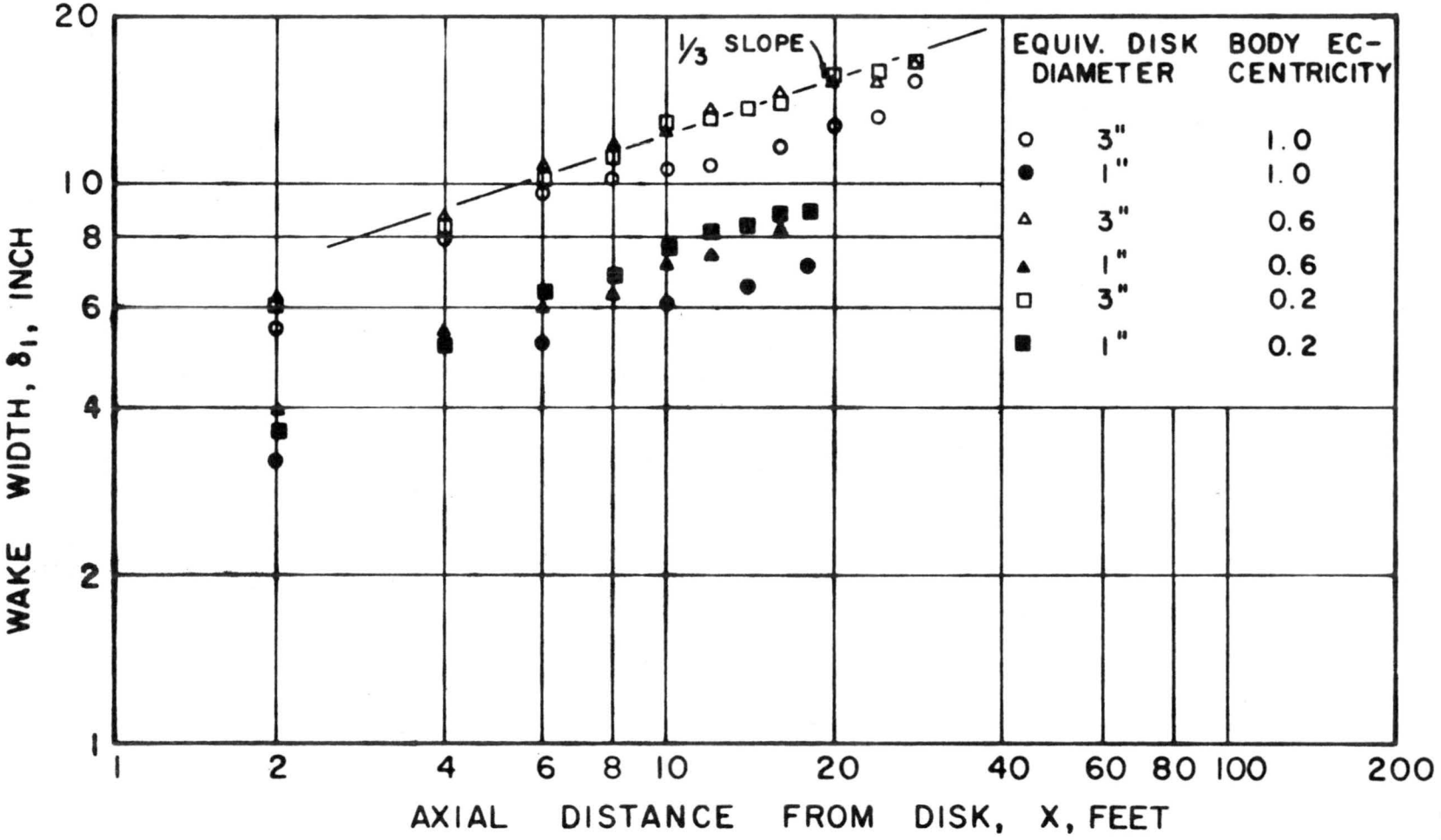

Figure 10. Wake Growth Along the Major Axis of the Wake.

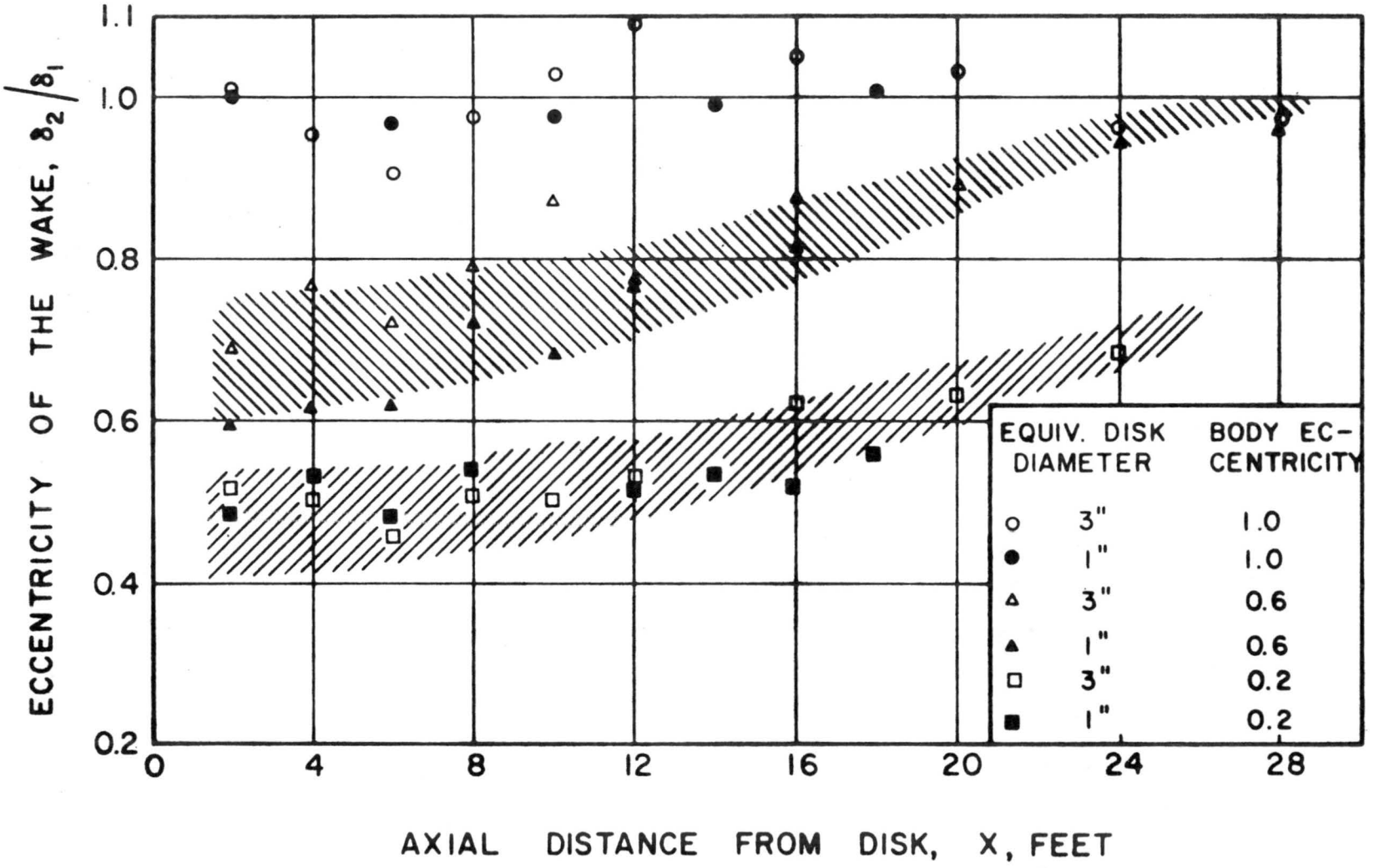

Figure 11. Variation of Eccentricity of the Wake in Axial Direction

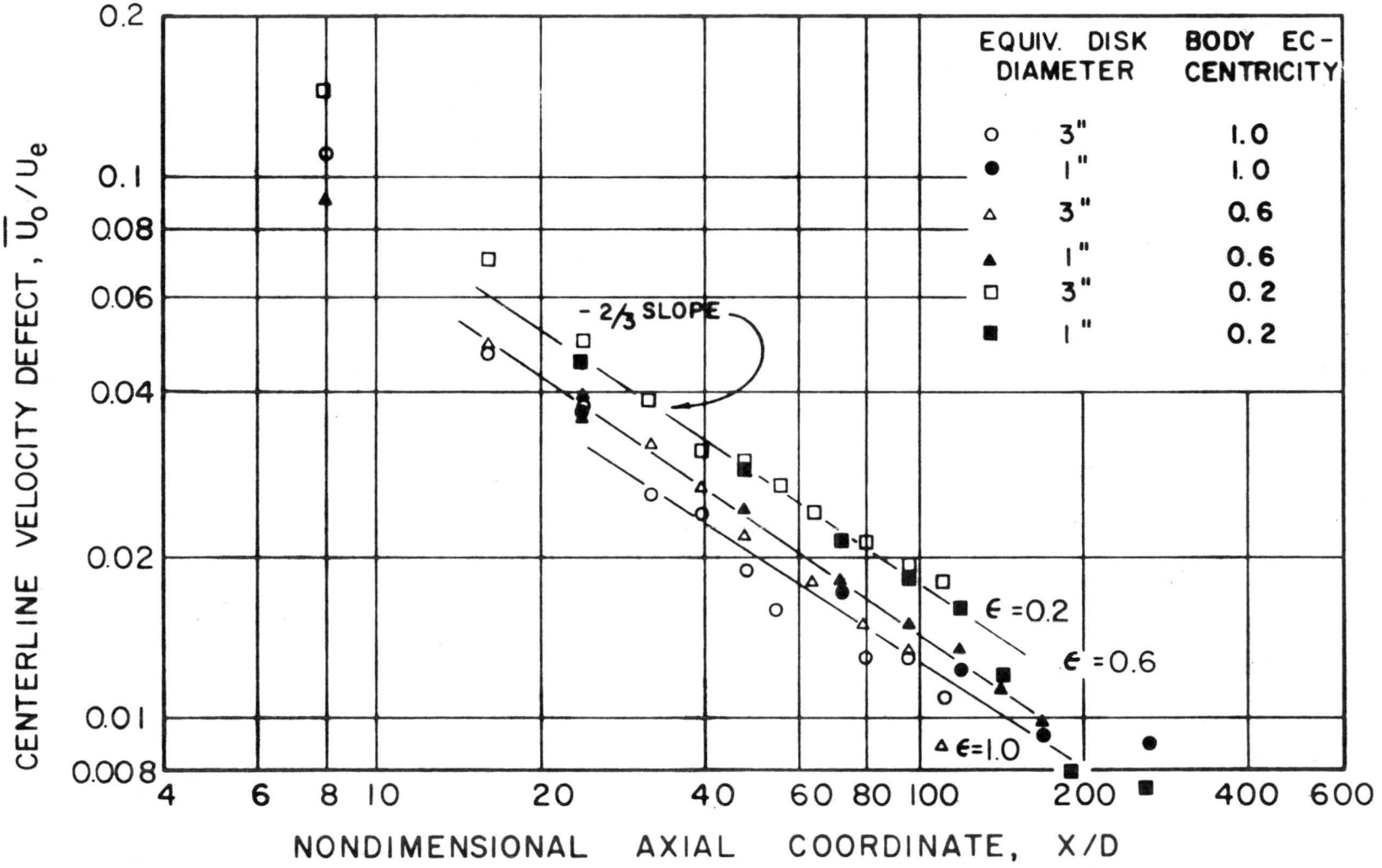

Figure 12. Variation of Velocity Defect Along the Axial Centerline.

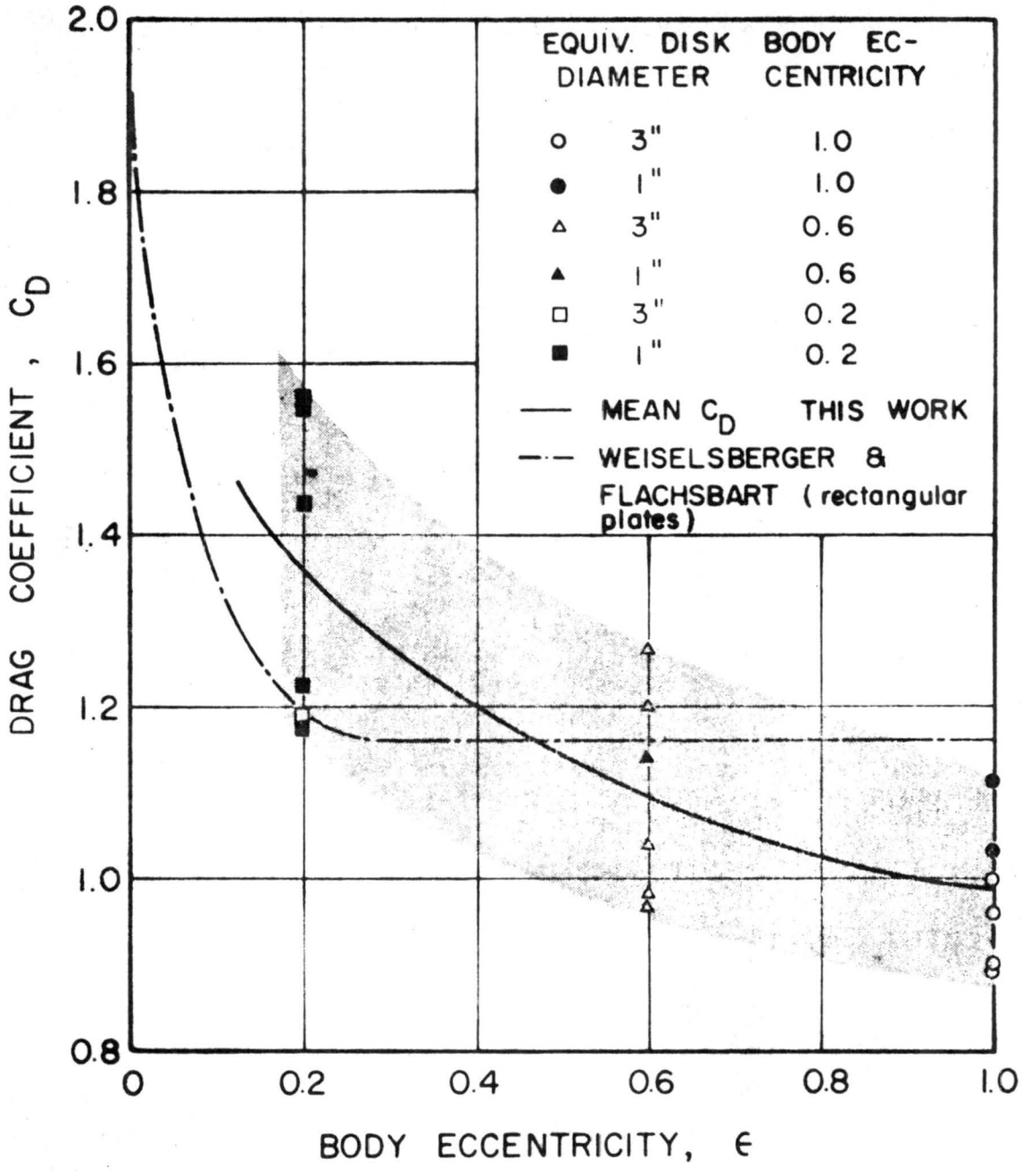

Figure 13. Drag Coefficient For Elliptical Disk Normal to the Flow (U_e = 58 ft/sec)

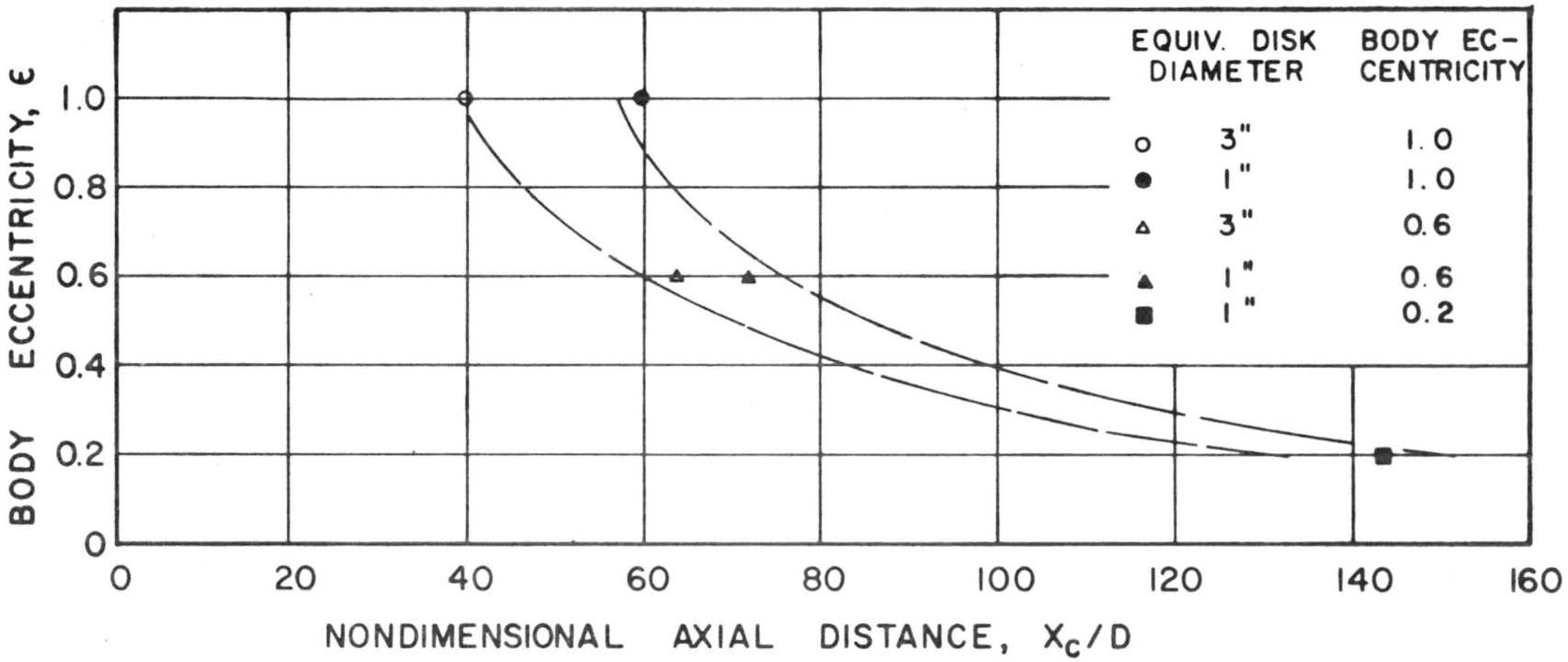

Figure 14. Effect of Body Eccentricity on "Initial Station" X_c

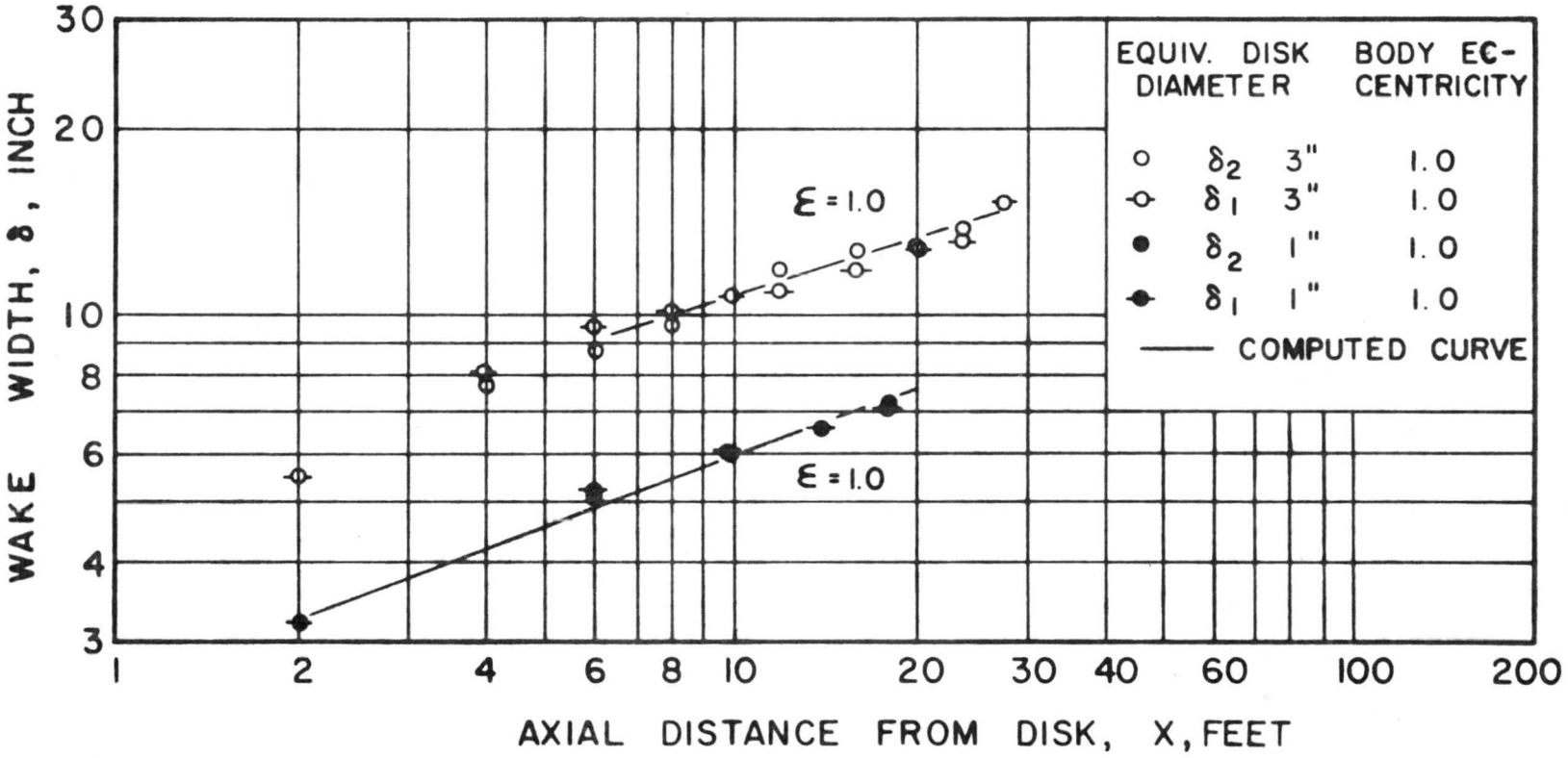

Figure 15. Comparison of Axial Variation of the Wake Widths with Analytical Predictions (ξ = 1.0.)

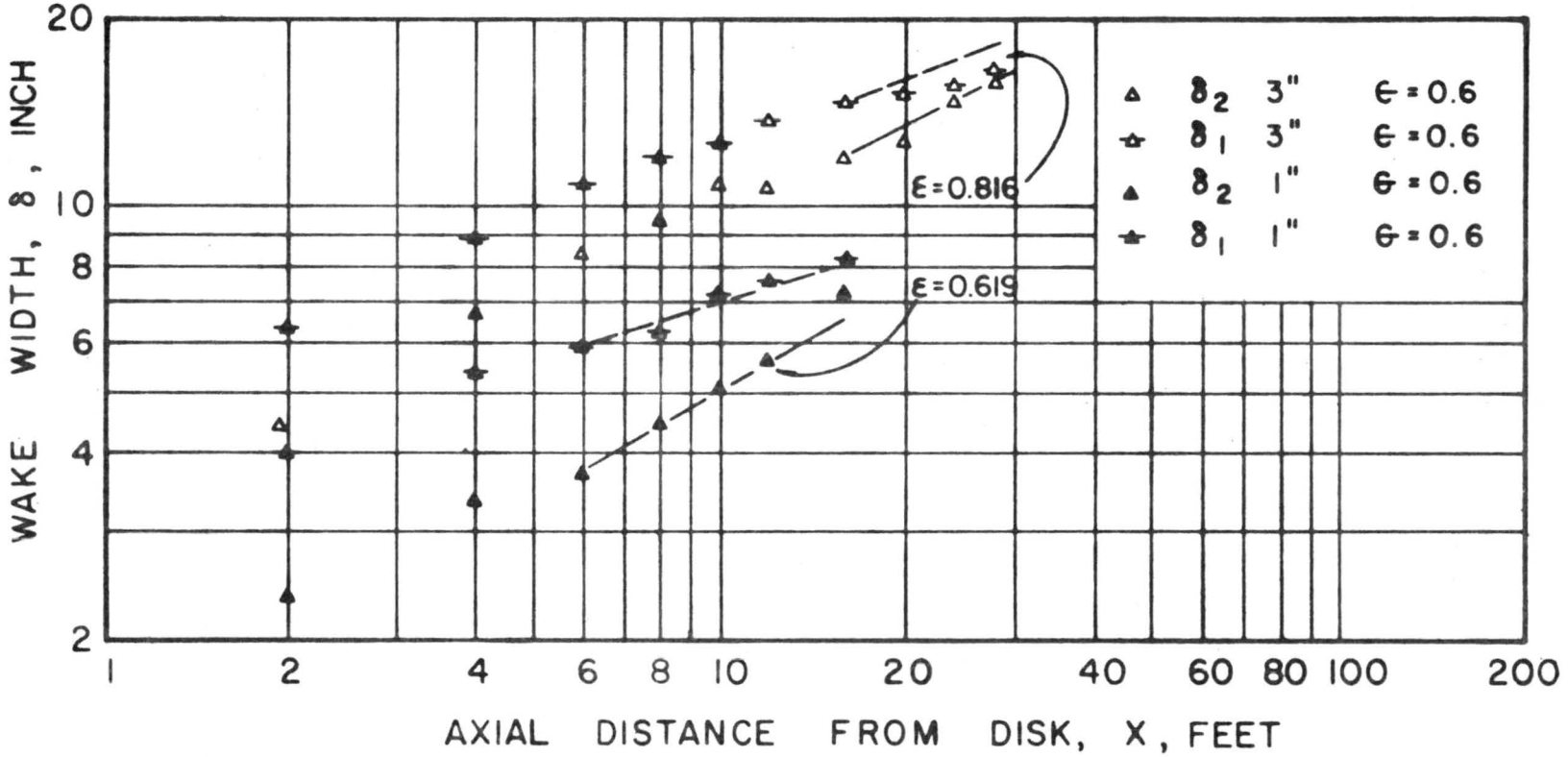

Figure 16. Comparison of Axial Variation of the Wake Widths with Analytical Predictions (ξ = 0.816, ξ = 0.619)

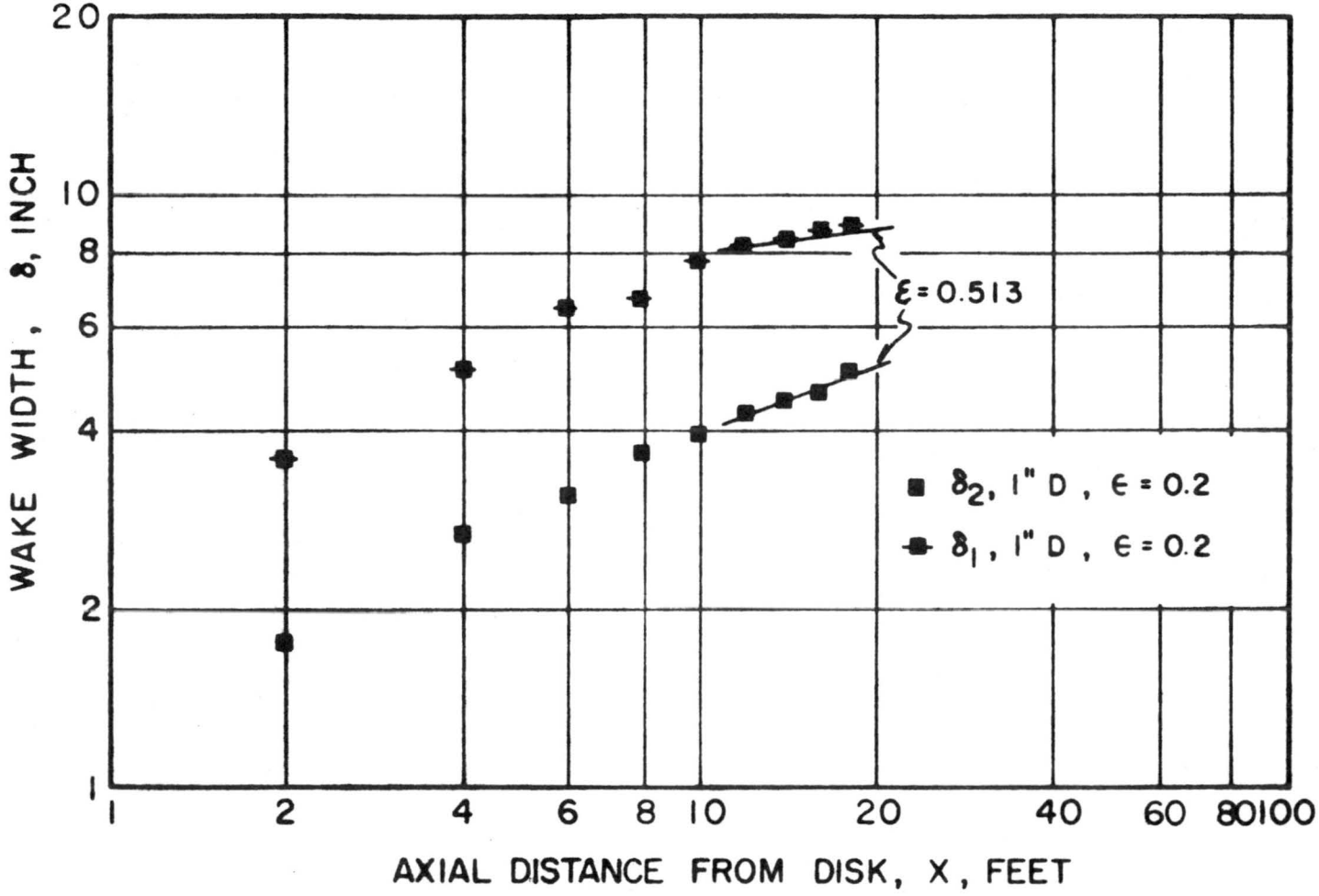

Figure 17. Comparison of Axial Variation of the Wake Widths with Analytical Predictions (ε = 0.513)

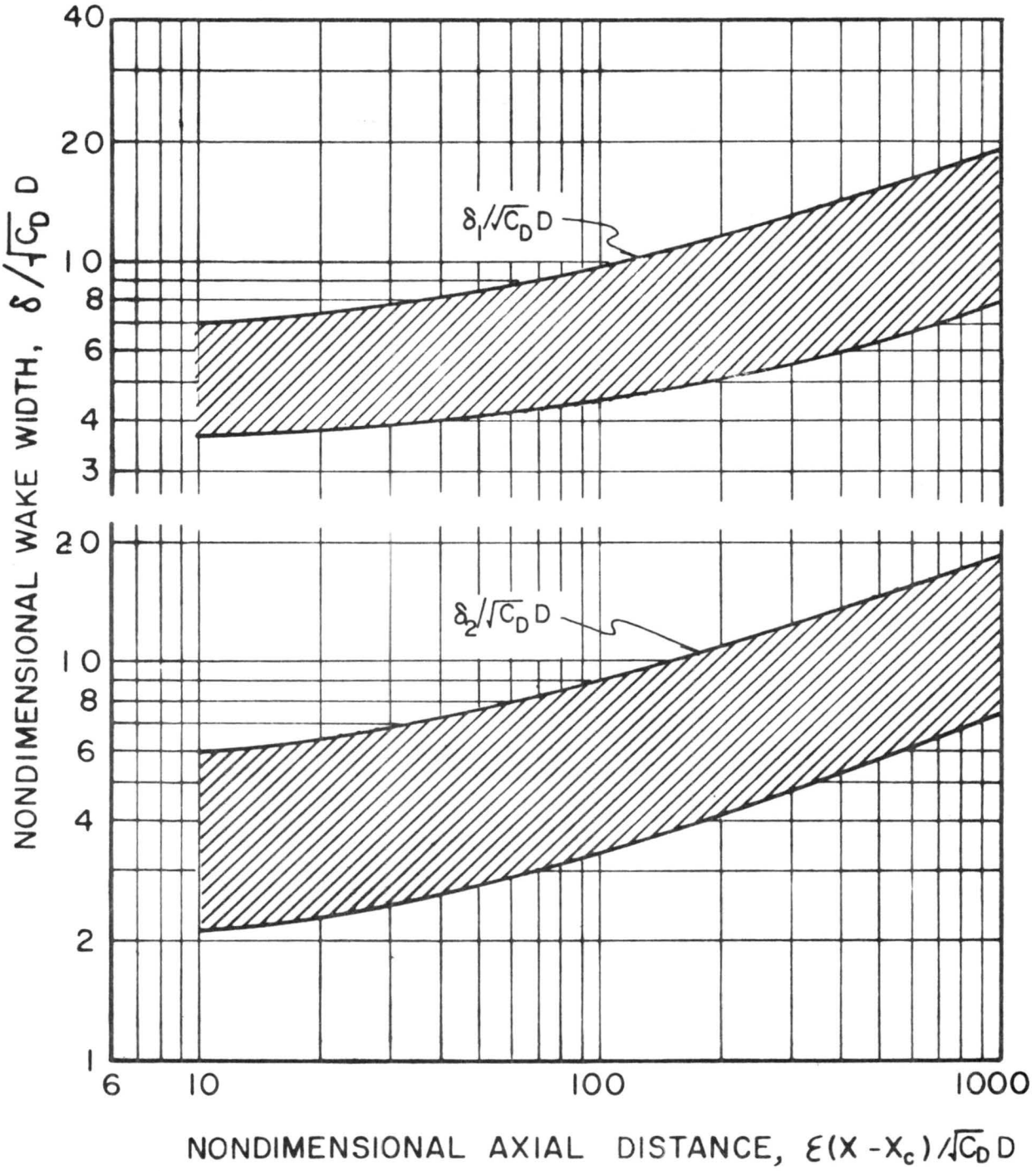

Figure 18. Predicted Non-dimensional Wake Growth

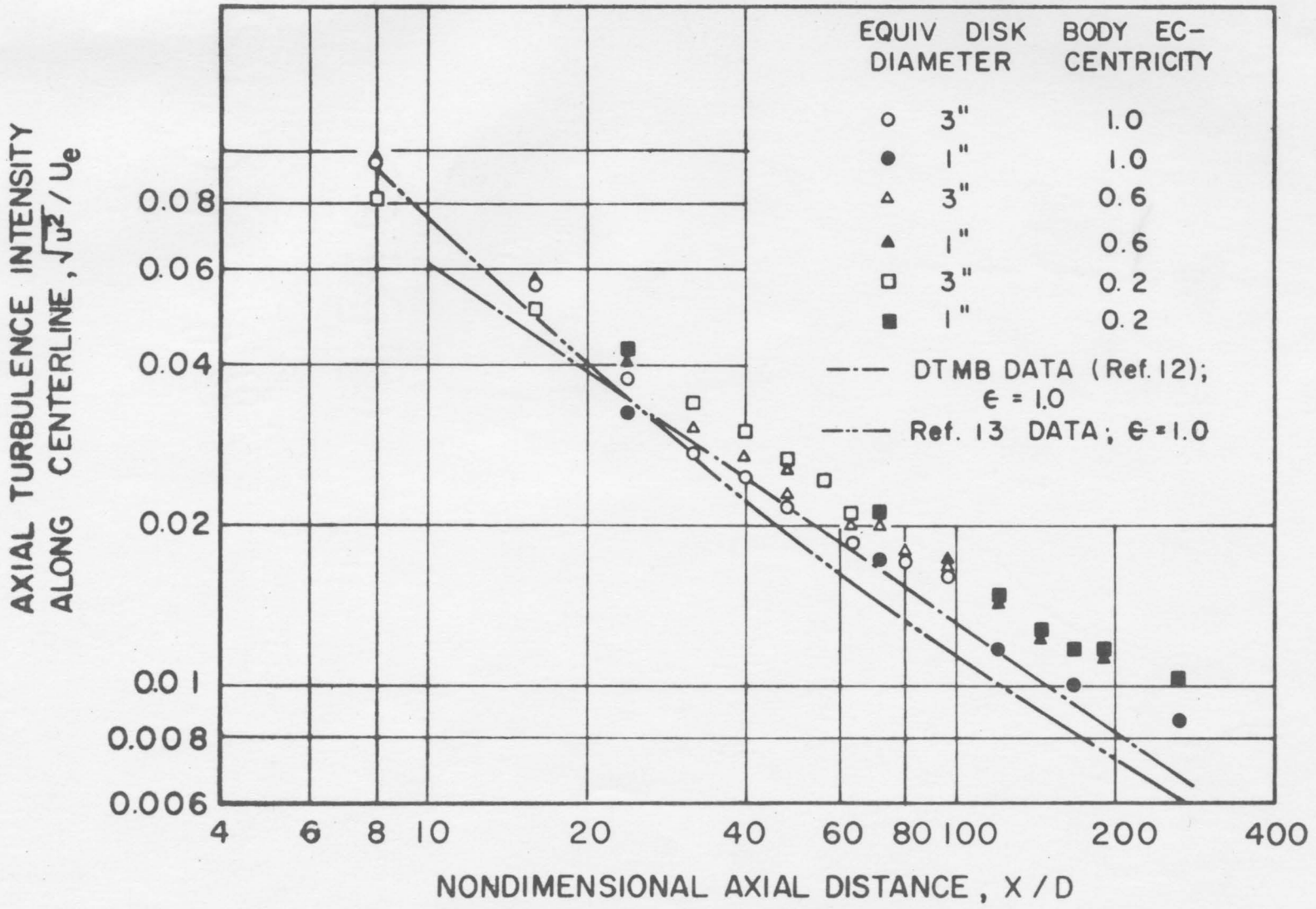

Figure 19. Variation of Turbulence Intensity Along the Axial Centerline of the Wake